ADVANCED MATERIALS

DOI: 10.1002/adma.200700011

A Strategy for Dimensional Percolation in Sheared Nanorod Dispersions**

By *Xiaoyu Zheng*, *M. Gregory Forest*,* *Richard Vaia*,* *Michael Arlen*, *Ruhai Zhou*

As the aspect ratio of a unit (here, a stiff high-aspect-ratio rod) increases, the tendency increases for ensembles of these units to form hierarchical structures on scales quite removed from that of the single unit (particles). This is due in large part to geometrical packing considerations (based on excluded volume analysis) arising from the non-spherical shape. Nematic ordering of rod ensembles[1] is one illustration of this phenomenon, and percolation of rod or platelet inclusions is another. It happens that for thin rods, equilibrium percolation of isotropic distributions occurs well below the nematic transition. The introduction of a flow-induced distribution function leads one out of the highly studied domain of universal scaling laws for equilibrium, isotropic percolation thresholds. For materials processing applications, one is compelled to explore the impact of volume fraction of particles beyond the threshold of any desirable percolation-induced property transition and ascertain the role of anisotropy on macroscopic property tensors. This is required for practical applications in order to avoid statistical fluctuations across the preferred side of the threshold.

There is a large quantity of literature on the onset of percolation among rods or "sticks" in two and three space dimensions, including seminal contributions of Balberg and collaborators[3,8,9], Bug et al.[2], Munson-McGee[10], Philipse[11], Celzard et al.[12], Neda et al.[13]. A key factor in all rigorous percolation analyses of thin rod ensembles is that the orientational distribution function can be approximated by a classical equilibrium distribution (random, Gaussian, Boltzmann, or a special separable form in spherical coordinates). Percolation thresholds for these special equilibrium distributions are intimately connected with universal scaling laws and self-similarity, and the scale-invariant nature of the behavior at threshold. These fundamental scaling laws have played a dominant role in providing the basis for estimates of property percolation thresholds due to spanning networks formed by percolating rod clusters; we note the recent analysis of Hu et al.[38] on nanowires in a poorly conducting medium. The thresholds are statistical in nature; for example, at some critical volume fraction, there is a finite probability that a spanning network cluster will form, and the cluster features will depend on the underlying lattice construct (e. g. triangular lattice, Bethe lattice, continuum, etc.)[28]. Anisotropic percolation arises when the percolation threshold depends on spatial direction, which in nanorod composites arises due to processing history[16].

In this paper, the departure from universality and self-similarity of the percolation thresholds is explored, associated with non-classical and non-equilibrium rod distribution functions arising from an imposed shear flow. There are no theoretical scaling results to rely upon for sheared distributions. Yet there is mounting evidence that a combination of shear rate, rod volume fraction and aspect ratio determine percolation thresholds in stiff-rod composites (Ounaies et al.[15], Xu et al.[16], Lahiff et al.[17]). Although never completely characterized, the orientation distributions of the rods in these systems are probably non-classical and are far from equilibrium due to processing procedures. Thus, ascertaining the interrelationships between processing (shear rate) and composite composition (volume fraction and aspect ratio of rods) is not straight forward. It should be noted that experimentally, percolation thresholds are often inferred by measuring sharp jumps in conductivity, rather than by actual rod-rod contact percolation. This identification introduces an uncontrollable error into contact percolation prediction since property percolation (e. g. conductivity) occurs prior to contact percolation via processes such as electron tunneling and carrier hopping. This effect, which is dependent on details of the particular structure, also leads to non-universality of critical exponents in conductive percolation scaling laws (Grujicic et al.[18], Vionnet-Menot et al.[19], Heaney[20]).

Clearly, there is a gap between universal scaling laws derived from rigorous percolation analysis and the percolation

[*] Prof. M. G. Forest
Department of Mathematics & Institute for Advanced Materials
University of North Carolina at Chapel Hill
E-mail: forest@amath.unc.edu
Dr. R. Vaia, Dr. M. Arlen
Air Force Research Laboratory, Wright-Patterson AFB
E-mail: richard.vaia@wpafb.af.mil
Prof. X. Zheng
Department of Mathematical Science, Kent State University
Prof. R. Zhou
Department of Mathematics and Statistics,
Old Dominion University

[**] We acknowledge helpful conversations with Prof. Richard Smith, Department of Statistics, UNC-CH. Effort sponsored by the Air Force Office of Scientific Research, Air Force Materials Command, the Intelligence Community (IC) Postdoctoral Program (USA)F grant F49620-6-0088, the National Science Foundation through grants 0406374, 0604891, 0604912, and the Army Research Office, under grant number W911NF-04-D-0004. This work is supported in part by the NASA University Research, Engineering and Technology Institute on Bio Inspired Materials (BIMat) under award No. NCC-1-02037.

thresholds arising in sheared rod systems. Recent attempts to fill this gap have relied upon ad hoc assumptions about the probability distributions. In Natsuki et al.[21], instead of random planar orientation angles for 2d rod systems, the authors prescribe a top-hat PDF which is zero outside of a wedge, and random inside the wedge of angles. They then demonstrate 2d percolation thresholds vary with such anisotropic distributions. The strategy presented is similar in spirit to ours, with notable differences: consideration of 3d nanorod systems; and the orientational probability distribution functions (PDFs) are not posited, rather they are computed from Doi-Hess kinetic theory. Prior work by the authors has derived an asymptotic description of shear-induced nanorod orientational distribution functions[14], confirmed by high-resolution numerical solutions[33,34]. This yields a numerical description for sheared nanorod macromolecular dispersions, which captures the coupling between excluded volume, rotational diffusion, and shear flow. A Monte Carlo (MC) population algorithm and a search algorithm are then implemented, yielding a *parameter continuation of universality-based percolation thresholds into the non-equilibrium regime of sheared percolation thresholds*. In this regime, shear flow "shapes" distributions with anisotropy relative to the flow geometry, and the coupled algorithms demonstrate that percolation thresholds become directional, yet are controlled by volume fraction and shear rate.

These anisotropy/dimensional characterizations of percolation thresholds follow the authors' earlier volume-averaged characterizations of conductive[22,23] and mechanical anisotropy[24] in sheared nanorod dispersions. These homogenization results give coarse-grained properties that depend only on the second moment (for conductivity tensors), or second and fourth moments (for mechanical tensors), of the nanorod PDF. These predictions do not account for percolation in the nanorod ensemble, and thus will miss the sharp and dramatic jumps in properties due to physical percolation.

Similar morphology-transport correlations can be found in diverse fields, ranging from ground water permeation (clays have highly anisotropic microstructure), to dielectric breakdown, to fracture of composite plies. Of particular interest for the present paper is the area of polymer nanocomposites. Dispersions of nanoparticles, including carbon nanotubes, nanoclays, oxide nanoribbons and metallic nanorods, have demonstrated exciting opportunities for high-end, multifunctional applications, as well as enabling never-before-realized materials with unique combinations of electrical, optical, and structural properties[25]. Reinforcement, as well as transport dominated properties such as electrical conductivity, are intimately related to the hierarchical network architecture of these anisotropic nano-units. The references above all provide evidence of this realization, and the various approaches to build a set of predictive tools. These extended scale properties of the ensemble of nano-particles are highly dependent on process history and are rarely isotropic[26,27]. Predictive tools for the correlation between the characteristics of the network (e. g. volume fraction of rods, distribution of size and shape of rods, and orientational distribution, both local and global, of rods), processing history, and the anisotropy of the macroscopic properties, are critical to engineering these responses.

The strategy presented involves three steps. The first step is a computation of the non-equilibrium orientational probability distribution function (PDF) of Doi-Hess theory for flowing rigid-rod macromolecules in a viscous solvent[5,6]. This theory provides a Smoluchowski equation for the PDF of the rod ensemble, whereby viscous Stokes flow of a spheroid is coupled to an excluded-volume potential for the particle–particle interactions, and rotational diffusion of each rod. The flow is imposed for this first study, namely in terms of simple shear with a prescribed shear rate. This assumption decouples the hydrodynamic equations and further assumes the PDF is homogeneous in space. This model is thereby relevant to so-called monodomains of nanorods in a viscous solvent which are on the order of a micron length scale. On scales above this one, spatial gradients in the PDF are inescapable. This monodomain study is prerequisite to the next step of percolation in macroscopic heterogeneous nanorod dispersions, this PDF solution algorithm is explained in detail in Forest et al.[33,34].

In the second step, Monte Carlo samples are populated by drawing from the Doi-Hess-Smoluchowski PDF which encodes the particle geometry and volume fraction, flow type and rate. Note that the preponderance of results in the literature are based on Monte Carlo (MC) simulations[8,9,29,30,31,32]. The MC statistical approach employed here differs by the class of distribution functions used, and the way in which we populate the nanorod phase within the composite.

The third step is a data-mining algorithm applied to the MC realizations, from which it is determined whether each nanorod ensemble contains a percolating cluster in either of the flow-flow gradient-vorticity physical dimension. When 50 % of the MC samples percolate, statistical percolation is declared; it is confirmed that this arbitrary 50 % criterion can be relaxed without significant changes in the percolation thresholds. Anisotropic percolation is easily identified by the "continuation method", analogous to bifurcation algorithms in standard software such as AUTO[36]. Namely, simulations begin from the equilibrium percolation threshold of isotropic nanorod distributions, where the results are benchmarked with seminal results of Balberg and collaborators. Parameter continuation versus imposed shear rate is performed until the percolating clusters fail to span the flow gradient direction, then at higher rates fail to span the vorticity direction, and finally fail to span the flow direction. Likewise, at fixed shear rate, volume-fraction continuation leads to analogous dimensional percolation thresholds. The multi-parameter continuation algorithm combines to determine "dimensional percolation phase diagrams". Note that the sequential loss of percolating clusters in directions relative to the flow geometry is intuitive, and indeed almost obvious. This strategy should be considered as a toolkit to guide and control dimensional percolation for nanorod macromolecular dispersions. Herein, this control

ADVANCED MATERIALS

strategy is illustrated for a 3 parameter space of shear rate, nanorod aspect ratio and volume fraction.

The percolation model presented is continuum (off-lattice) and permeable (soft core) as in Balberg et al. (1984)[9]. The PDFs from Doi-Hess kinetic theory resolve rotational diffusion, excluded volume, rod aspect ratio, and hydrodynamic interactions arising in an imposed rheological flow (simple shear is explored here). The excluded volume potential is a mean-field potential which does not address the pair-wise particle interactions. As a result, if one draws from the PDF of the mean-field theory, particles will overlap with finite probability unless new physics is added to remove or prevent overlap. Either one has to pass down to a particle molecular dynamics code to remove overlaps (a starting point might be the approach of Grujicic et al.[18]), or one might invent some ad hoc rules at the PDF level. Since the overlap volume fraction is exceedingly small, the PDF proceeds without addressing the issue of overlap for this study; and the authors refer to the recent study of CNT-polymer composites which do not take overlap into account[37], yet consider a piecewise linear model of fiber flexibility. Specifically, our algorithm proceeds as follows.

The sample used for the study is a cubic box with fixed length L. The particles are idealized as monodisperse soft-core spheroids, represented as a cylinder plus two spherical caps, with length l and diameter d. For random orientational distributions with overlapping particles allowed, the actual volume fraction occupied, θ, is given in terms of single particle volume V and the number density n of particles by Balberg (1986)[35]

$$\theta = 1 - \exp(-nV), \tag{1}$$

which of course is different from the obvious formula when the particles are impenetrable: $\theta = nV$. The Balberg formula is then utilized to calculate the number N of particles in the cube of volume L^3:

$$N = \frac{ln(1-\theta)^{-1}L^3}{V}. \tag{2}$$

In this cube, sites are "planted" with random coordinates $(x_i, y_i, z_i)(i = 1,\cdots N) \in [0,L]^3$. To each site (x_i, y_i, z_i), a rod is attached with length, l, diameter, d, and orientation $(u_i, v_i, w_i) \equiv \mathbf{m} \in S^2$, chosen by drawing from the orientational probability distribution function f. Periodic boundary conditions are used here, which is implemented by putting images of each rod in the corresponding 2 neighboring identical boxes, the positions of the neighboring boxes are determined by the direction of interest. Since some rods are partially out of the box, an additional rod image will be added to the opposite boundary of the box, such that correct particle volume fractions are obtained. Initially, each rod is assigned a unique cluster number.

To accelerate simulations, the box is divided into uniform bins, whose length equals the rod length. For a nonzero width rod, it may reside in at most 8 neighboring bins. Next, the connectedness of each rod with all neighboring rods in the bins it resides is checked. If rods are "connected", the minimum of their cluster numbers is assigned as their common cluster number. This way, small cluster numbers prevail. Connectedness is determined by checking the distance between two rods. If the distance is less than or equal to the rod diameter, the two rods are considered connected.

Finally, a percolating cluster is identified when rods in boundary bins on *opposite sides of the cube* have common cluster number(s). If no percolating cluster is identified, the volume fraction of the rods is increased, and the above steps repeated. For each PDF from the Smoluchowski equation, 100 realizations are created, and 50 % of these samples are required to have a spanning (percolating) cluster to declare a percolation threshold.

A sample rod dispersion drawn from a random orientation distribution, $f \equiv 1/4\ \pi$, of 1 nm × 50 nm rods at 0.01 vol % is shown in Figure 1a, with a blow-up of one thousandth of the full box shown in Figure 1b. A representative percolating cluster identified by the algorithm above is shown in Figure 1c, where the total number of rods $N = 60\,000$ and the percolating cluster contains ~ 8 % of the rods.

The apparently arbitrary trigger point of 50 % of the samples to declare a percolation threshold is rationalized in Figure 2. The critical volume fraction θ_p is based on the 50 % MC sample criterion, for 3 different aspect ratio dispersions ($r = 100, 200, 500$). Figure 2 shows the percentage of MC samples that yield a percolating cluster drops off rapidly below θ_p and increases rapidly above θ_p. When the trigger point is set to 25 % or 75 %, the critical threshold θ_p will vary, but not significantly. The percentage of percolating clusters around the 50 % threshold sharpens at higher aspect ratios, consistent with critical transition phenomena.

The scaling of θ_p with particle aspect ratio r is depicted in Figure 3. Results demonstrate $\theta_p = 0.037$ for $r = 20$, then θ_p drops rapidly to $\theta_p = 0.0065$ for $r = 100$ and $\theta_p = 0.0012$ for $r = 500$. Then the suggestion in Bug et al. (1985)[2] to fit these data using

$$\theta_p = \frac{C_1}{r} + \frac{C_2 \log r}{r^2}, \tag{3}$$

and demonstrates good agreement for all aspect ratios. The theory in Balberg et al. (1984)[3] (that the percolation threshold is proportional to reciprocal excluded volume) suggests a scaling law

$$\theta_p \propto \frac{V}{\langle V_{ex} \rangle} \propto \frac{1}{r} \tag{4}$$

Although this is valid for extremely large aspect ratios $r \to \infty$, it does not adequately describe the behavior for aspect ratios considered here (10–10^3).

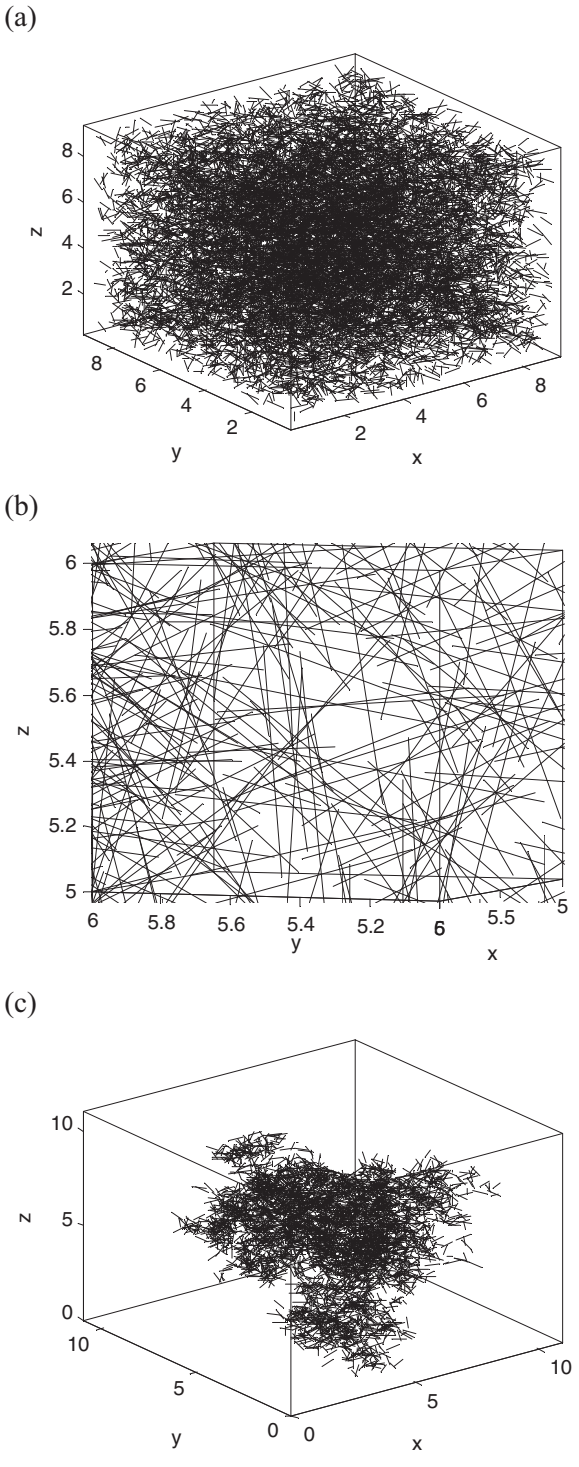

Figure 1. (a) $(1\,\mu m)^3$ sample of 1 nm × 50 nm rods at 0.01 vol %. (b) A blow-up of the left Figure in a $(100\ nm)^3$ subset. (c) A percolating path with all side branches of nanorods in contact.

The impact of anisotropic non-equilibrium rod distributions is now considered, which is described by PDFs consistent with the flow history of the nanorod ensemble. Simulations are initiated at volume fractions below the nematic transition, since

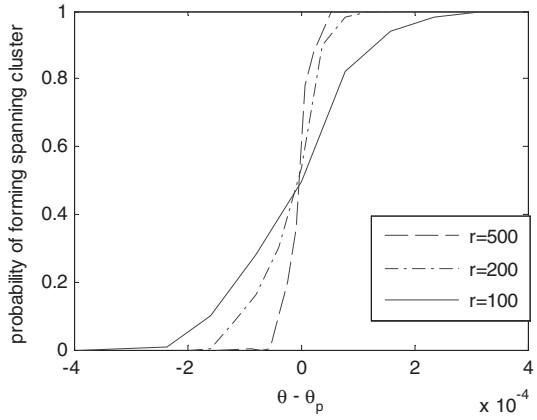

Figure 2. Probability of MC samples which yield a spanning cluster for volume fractions near the 50 % criterion for percolation threshold θ_p. These statistics are computed for random PDFs of nanorod dispersions with aspect ratios $r = 100,200,500$.

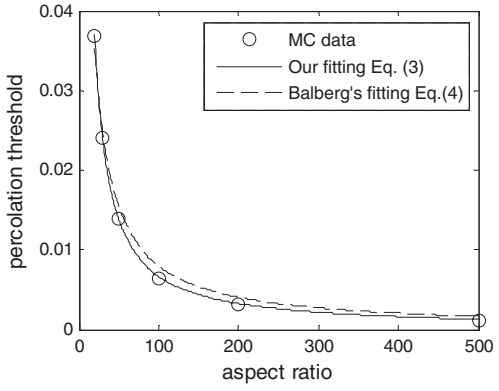

Figure 3. Percolation threshold volume fraction θ_p vs. aspect ratio for random orientational distributions of nanorods. We compare our fitting with Balberg et al. (1984) [3].

the onset of percolation occurs within the isotropic phase for any sufficiently large aspect ratio ($r > 30$ in our simulations). At these concentrations, isotropic PDFs are "shaped" by an imposed flow type and rate. For illustration, consider pure shear with variable shear rate and rod aspect ratio $r = 50$. The above algorithms are implemented using our Doi-Hess-Smoluchowski algorithm for each PDF versus variable normalized shear rate (Peclet number, Pe) and volume fraction; the results for directional percolation thresholds are shown in Figure 4.

Figure 4 is a "percolation phase diagram" capturing percolation thresholds in the 2-parameter space of volume fraction and normalized shear rate. Above the solid curve, percolating clusters span all 3 directions; between the dashed and solid curves, percolating clusters span flow (x) and vorticity (z) directions, without percolation along the flow gradient (y) direction; between the dashed and dash-dot curves, percolating clusters span the flow direction (x) only; below the dash-dot curve, percolation is statistically lost. These results are consis-

ADVANCED MATERIALS

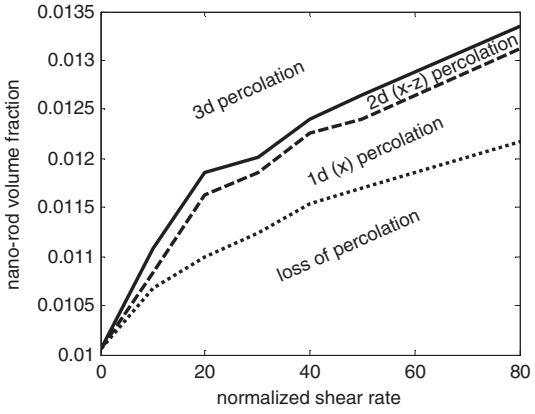

Figure 4. "Percolation phase diagram" of anisotropic percolation thresholds versus critical volume fraction θ_p and normalized shear rate Pe, for monodisperse rods of aspect ratio 50. The three curves indicate the directional percolation transition relative to the flow-flow gradient-vorticity axes. Above each curve, percolation is gained in that dimension, so the diagram reads from bottom to top or right to left: 0d, 1d, 2d, and then 3d percolation.

tent with the experimental observations of time-dependent conductivity transitions in sheared CNT suspensions in Xu et al.[16], as follows. These PDFs are steady-state attractors of the Doi–Hess–Smoluchowski equation, so they correspond to long-time data from Xu et al.[16]. Indeed, Figure 4 predicts processing regimes where prior to shear, percolation is 3d leading to extremely high conductivity in all directions, and then shear processing leads to loss of percolation and corresponding precipitous decrease in conductivity in all directions. This precise scenario is reported in Figure 3 of Xu et al.[16].

Figure 5 depicts exemplary percolating paths at the right vertical boundary (Pe = 80) of Figure 4. A similar scenario to Balberg et al. (1984)[9] is found, where they modify the orientational anisotropy in an *ad hoc* manner by limiting the azimuthal angle θ and polar angle ϕ in controlled intervals; analogous trial PDFs are considered by Natsuki et al.[21]. By contrast, the PDF presented computes the probability density function $f(\theta, \phi)$ everywhere on the sphere by solving the Doi-Hess-Smoluchowski equation. In Balberg's approach, for each specified orientational distribution, the critical volume fraction is found by continually adding rods to the system until a percolating path forms. In contrast, the orientational distribution functions utilized here are functions of volume fraction and shear rate. Thus at a fixed shear rate, when the volume fraction of nano-particles is increased, all other particles in the system are influenced, and a completely new PDF is recomputed to generate the MC statistics. Overall, both approaches confirm that random PDFs have lower percolation threshold volume fractions than a non-random PDF with the same particle geometry.

The results presented above, summarized in Figures 4 and 5, imply that *a combination of shear rate* and *volume fraction can be used to control dimensional percolation in shear-processed*, *nanorod composite films*. Numerous applications, including smart materials, piezo- and pyro-resistive sensors

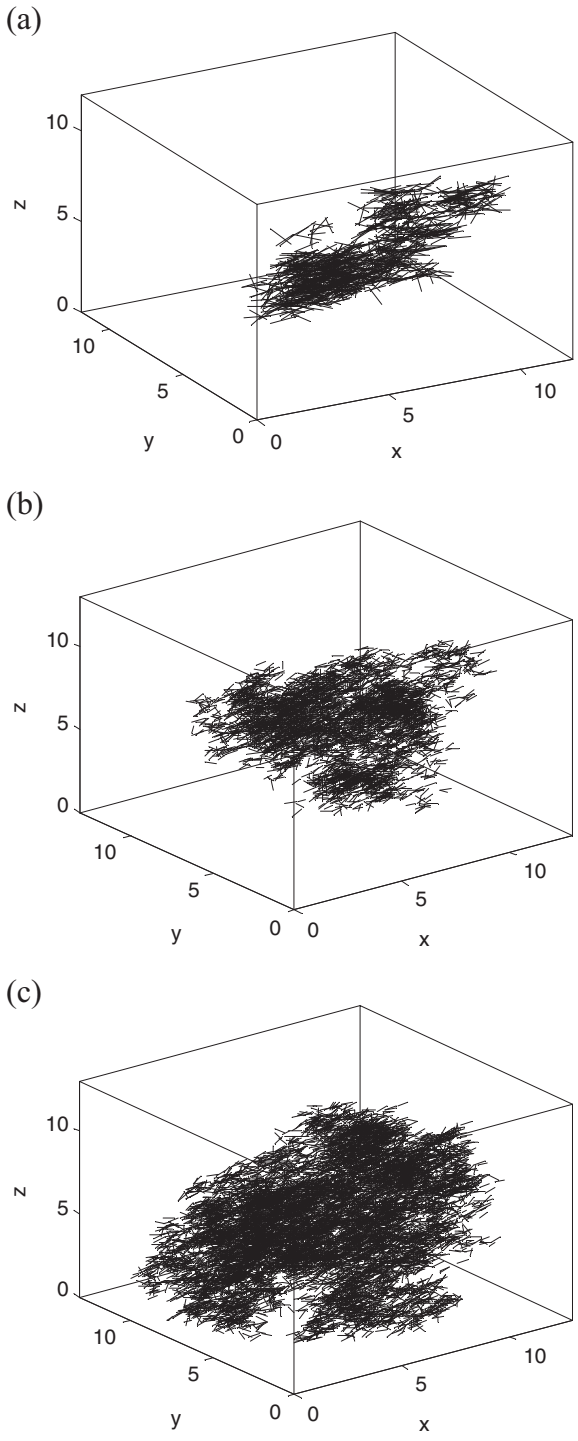

Figure 5. Anisotropic percolation versus volume fraction at a fixed high shear rate (Pe = 80). (a) 1d percolation, with percolation paths spanning only the flow (x)-direction, with $\theta_p^{(x)} = 0.012$; (b) 2d percolation, with percolating paths now spanning the vorticity (z) direction as well as flow direction with $\theta_p^{(x,z)} = 0.0131$; (c) 3d percolation, with percolating paths now also spanning the flow gradient (y) direction, with $\theta_p^{(x,y,z)} = 0.0134$.

and actuators, are enabled by the controllable production of nanocomposite films with anisotropic conductivity (parallel or perpendicular to the surface of the film). Elucidating the

dependence of transitions between 3d, 2d, 1d percolating nanorod structures on global orientational distribution functions of the rod phase is necessary for further development of quantitative structure-performance relationships for these nanocomposite applications. The recent experimental study of anisotropic percolation in sheared carbon nanotube composites[16] is an example of the phenomenon that is predicted here. Furthermore, an algorithmic strategy for Brownian nanorods dispersed in a solvent and subjected to shear processing is presented, focusing in this paper on monodomains. The strategy combines three algorithms: generation of PDFs from the Doi-Hess-Smoluchowski equation for flowing macromolecules with an excluded-volume potential; a Monte Carlo algorithm that generates realizations of the post-processed rod-matrix composite from the orientational probability distribution function of the rod ensemble; and a data mining algorithm to determine percolation thresholds in all 3 physical dimensions of the nanorod phase. Although the tools presented are applied to identify percolation thresholds of anisotropic, non-equilibrium nanorod dispersions, they are equally applicable far from threshold conditions. The next step in this study is to extend these monodomain long-wavelength-limit calculations of the percolation phenomena to heterogeneous dispersions where macroscopically a film may be comprised of a spatially varying PDF.

Received: January 2, 2007
Revised: March 23, 2007
Published online: October 31, 2007

[1] L. Onsager, *Ann. NY. Acad. Sci.* **1949**, *51*, 627 .
[2] A. L. R. Bug, S. A. Safran, I. Webman, *Phys. Rev. Lett.* **1985**, *54*, 1412.
[3] I. Balberg, C. H. Anderson, S. Alexander, N. Wagner, *Phys. Rev. B* **1984**, *30*, 3933.
[4] M. Doi, S. F. Edwards, *The Theory of Polymer Dynamics*, Oxford University Press, Oxford, UK **1986**.
[5] S. Hess, *Z. Naturforsch. Teil.* **1976**, *31A*, 1034.
[6] M. Doi, *J. Polym. Sci., Polym. Phys. Ed.* **1981**, *19*, 229.
[7] G. B. Jeffery, *Proc. R. Soc., London A* **1922**, *102*, 161.
[8] I. Balberg, N. Binenbaum, *Phys. Rev. B* **1983**, *28*, 3799.
[9] I. Balberg, N. Binenbaum, N. Wagner, *Phys. Rev. Lett.* **1984**, *52*, 1465.
[10] S. H. Munson-McGee, *Phys. Rev. B* **1991**, *43*, 3331.
[11] A. P. Philipse, *Langmuir* **1996**, *12*, 1127.
[12] A. Celzard, E. McRae, C. Deleuze, M. Dufort, G. Furdin, J. F. Mareche, *Phys. Rev. B* **1996**, *53*, 6209.
[13] Z. Neda, R. Florian, Y. Brechet, *Phys. Rev. E* **1999**, *59*, 3717.
[14] M. G. Forest, R. Zhou, Q. Wang, *J. Non-Newtonian. Fluid Mech.* **2004**, *116*, 183.
[15] Z. Ounaies, C. Park, K. E. Wise, E. J. Siochi, J. S. Harrison, *Compos. Sci. Technol.* **2003**, *63*, 1637.
[16] J. Xu, W. Florkowski, R. Gerhardt, K. Moon, C. Wong, *J. Phys. Chem. B* **2006**, *110*, 12 289.
[17] E. Lahiff, R. Leahy, J. N. Coleman, W. J. Blau, *Carbon* **2006**, *44*, 1525.
[18] M. Grujicic, G. Cao, W. N. Roy, *J. Mater. Sci.* **2004**, *39*, 4441.
[19] S. Vionnet-Menot, C. Grimaldi, T. Maeder, S. Strassler, P. Ryser, *Phys. Rev. B* **2005**, *71*, 064 201.
[20] M. B. Heaney, *Phys. Rev. B* **1995**, *52*, 12 477.
[21] T. Natsukia, M. Endo, T. Takahashi, *Phys. A* **2005**, *352*, 498.
[22] X. Zheng, M. G. Forest, R. Lipton, R. Zhou, Q. Wang, *Adv. Funct. Mater.* **2005**, *15*, 627.
[23] M. G. Forest, X. Zheng, R. Zhou, Q. Wang, R. Lipton, *Adv. Funct. Mater.* **2005**, *15*, 2029.
[24] X. Zheng, M. G. Forest, R. Lipton, R. Zhou, *Continuum Mech. Thermodyn.* **2007**, *18*, 377.
[25] R. A. Vaia, H. D. Wagner, *Materials Today* **2004**, *7*, 38.
[26] A. A. Gusev, M. G. Rozman, *Comp. Theor. Poly. Sci.* **1999**, *9*, 335.
[27] A. A. Gusev, H. R. Lusti, *Adv. Mater.* **2001**, *13*, 1641.
[28] D. Stauffer, A. Aharony, *Introduction to Percolation Theory*, Taylor and Francis Ltd, London **1994**.
[29] G. E. Pike, C. H. Seager, *Phys. Rev. B* **1974**, *4*, 1421.
[30] N. Ueda, M. Taya, *J. Appl. Phys.* **1986**, *60*, 459.
[31] S. F. Wang, A. A. Ogale, *Compos. Sci. Technol.* **1993**, *46*, 379.
[32] M. O. Saar, M. Manga, *Phys. Rev. E.* **2002**, *65*, 056 131.
[33] M. G. Forest, Q. Wang, R. Zhou, *Rheol. Acta* **2004**, *43*, 17.
[34] M. G. Forest, Q. Wang, R. Zhou, *Rheol. Acta* **2004**, *44*, 80.
[35] I. Balberg, *Phys. Rev. B* **1986**, *33*, 3618.
[36] E. J. Doedel et al., AUTO97: Continuation and bifurcation software for ordinary differential equations, Concordia University **1997**.
[37] F. Dalmas, R. Dendievel, L. Chazeau, J. Y Cavaille, C. Gauthier, *Acta Mater.* **2006**, *54*, 2923.
[38] T. Hu, A. Grosberg, B. Shklovskii, *Phys. Rev. B* **2006**, *73*, 155 434.

